

Scanning Tunneling Spectroscopy Studies of High-Temperature Cuprate Superconductors

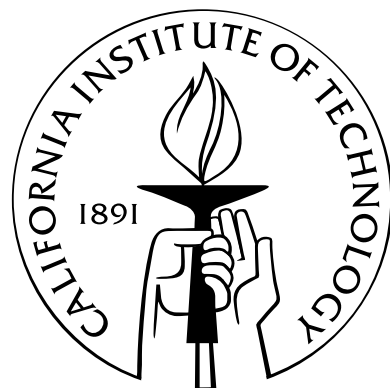
Thesis by

Ching-Tzu Chen

In Partial Fulfillment of the Requirements

for the Degree of

Doctor of Philosophy



California Institute of Technology

Pasadena, California

2006

(Defended May 19, 2006)

© 2006

Ching-Tzu Chen

All Rights Reserved

*To my parents
for their unconditional love and support*

Acknowledgements

This thesis would not have been completed without the help of many individuals. First of all, I would like to thank my advisor Professor Nai-Chang Yeh, for her guidance of my adventure into the vast high-temperature superconductivity field, for the enlightening discussions, her constant encouragement, and incomparable optimism despite frequent setbacks with instrumentation and fundings. Nai-Chang is unique in her comprehension and implementation of the theory that complements her experimentalist's intuition. Therefore, she has supported both the theoretical and experimental aspects of the thesis project, which makes this Ph.D. experience exceptional.

In the lab, I have been very fortunate to have "The Magician" Nils as a colleague and, more importantly, a great friend. Not only that the scanning tunneling microscope built for this thesis research would not have been realized without his expertise in the arts of machining, but also that I would not have learned so much more about life beyond physics. I am also thankful to Ted, for the interesting exchange of ideas, information and knowledge in science and culture; to Andy, for introducing me to both the techniques of cryogenic experiments and the American lifestyle outside the lab; to Andrew, for the fruitful collaboration I enjoyed during our endeavor into the phenomenological theory and for his great help with the experiments; to Cameron, for feeding me well with all sorts of homemade pastries and for sharing his passion toward the arts of cooking; to Slobodan and Marcus, for the witty discussions that show their terrific sense of dark humor; and to every Yeh group member for the friendship and support.

Aside from research, my life has been tremendously enriched by the numerous interesting friends whom I met in the States. Special thanks to Shing-Lin, for patiently listening to my (often immature) whining, providing to-the-point advice, and sharing her experience, wisdom, and philosophy; to

James, for his generosity and help in setting up the prototype interferometer; to Shao-Ching, for reaching out and helping me through the first two years at Caltech; to Hsin-Ying, for sharing the enthusiasm in physics; and to Hwa-Jen and Ivy, for all the fun discussions and the refreshing perspective on sociology and music.

Finally, I'd like to express my deepest gratitude to my parents, for their unconditional love and for letting me explore my interests and capability freely; to my best friend Yuan-Yu, for his companionship through the darkest period of my life; and to Pei-Ying, who can always bring a smile to my face.

Abstract

This thesis presents the scanning tunneling spectroscopic studies of the non-universal electronic properties among electron- and hole-doped cuprates. Tunneling spectra of the electron-doped $\text{Sr}_{0.9}\text{La}_{0.1}\text{CuO}_2$ and the hole-doped $\text{YBa}_2\text{Cu}_3\text{O}_{6+\delta}$ reveal distinctly different behavior in the pairing symmetries, pseudogap phenomena, satellite features, and low-energy excitations. While underdoped and optimally doped $\text{YBa}_2\text{Cu}_3\text{O}_{6+\delta}$ exhibits *d*-wave and overdoped Ca-doped $\text{YBa}_2\text{Cu}_3\text{O}_{6+\delta}$ (*d+s*)-wave pairing symmetry, the electron-doped $\text{Sr}_{0.9}\text{La}_{0.1}\text{CuO}_2$ shows fully gapped *s*-wave pairing symmetry. The absence of the satellite features and pseudogap in tunneling spectra of electron-doped cuprates sharply contrasts with their general presence in hole-doped cuprates. Furthermore, the subgap low-energy spectral characteristics of $\text{Sr}_{0.9}\text{La}_{0.1}\text{CuO}_2$ deviate substantially from the mean-field Bardeen-Cooper-Schrieffer theory, while those of $\text{YBa}_2\text{Cu}_3\text{O}_{6+\delta}$ can be fully accounted for by the mean-field generalized Blonder-Tinkham-Klapwijk formalism.

Despite the aforementioned disparities, several experimental results reveal important connections between the two types of cuprates. For instance, the coexistence of the pseudogap and superconducting spectra in hole-doped cuprates and the observations of the current- and field-induced pseudogap in electron-doped cuprates suggest that competing orders, manifested as the pseudogap, coexist with superconductivity in both types of cuprates. In addition, by comparing the tunneling spectra with the high-field vortex dynamics measurements, we find that the quasiparticle spectral characteristics of $\text{Sr}_{0.9}\text{La}_{0.1}\text{CuO}_2$ and $\text{YBa}_2\text{Cu}_3\text{O}_{6+\delta}$ correlate with the degree of field-induced quantum phase fluctuations of the two compounds.

Based on these findings, we propose a simple model of coexisting density waves with superconductivity to unify the apparent non-universal phenomena among cuprate superconductors. By

incorporating quantum phase fluctuations and adopting realistic band structures, numerical simulations of the quasiparticle tunneling spectra demonstrate excess subgap low-energy excitations, which is consistent with the empirical observations in $\text{Sr}_{0.9}\text{La}_{0.1}\text{CuO}_2$. Furthermore, by tuning the ratio of the density waves to superconductivity, the theoretical calculations reproduce the absence of pseudogap phenomena in electron-doped cuprates and the general presence of the pseudogap in hole-doped cuprates. Thereby, we conclude that the competing orders that coexist with superconductivity in cuprate superconductors contribute to the rich cuprate phenomenology.

Contents

Acknowledgements	iv
Abstract	vi
1 Introduction	1
1.1 Crystalline structures and electronic phase diagram of high-temperature superconductors	1
1.1.1 Crystalline and electronic structures of parent compounds	1
1.1.2 Electronic phase diagrams	3
1.1.3 Effective single-band Hubbard model and $t - J$ model	6
1.2 Electron-doped vs. hole-doped cuprates: review of current experimental and theoretical status	9
1.2.1 Pairing symmetry	9
1.2.2 Pseudogap	11
1.2.3 Orders in cuprate superconductors	15
1.3 Overview of the thesis	18
2 Physics of Tunneling Spectroscopy	21
2.1 Tunneling Hamiltonian	21
2.1.1 Normal-insulator-superconductor tunneling	26
2.2 Pairing symmetry and tunneling spectra: generalized Blonder-Tinkham-Klapwijk (BTK) model	30

2.2.1	Generalized Blonder-Tinkham-Klapwijk formalism—A mean-field description	32
2.2.2	Tunneling spectra of a <i>d</i> -wave superconductor and the Andreev bound state .	36
3	Scanning Tunneling Microscopy: Principle and Instrumentation	43
3.1	Brief review	44
3.2	Instrumentation of a cryogenic STM	46
3.2.1	STM head	47
3.2.2	STM electronics	50
3.2.3	Cryogenic probe and dewar	53
3.2.4	Noise reduction	56
3.3	Comparison with other experimental techniques	60
3.3.1	Tunneling spectroscopy	60
3.3.2	Angle-resolved photoemission spectroscopy	63
3.3.3	Neutron scattering	65
4	Tunneling Spectra of Hole-Doped $\text{YBa}_2\text{Cu}_3\text{O}_{6+\delta}$	67
4.1	Introduction	67
4.2	Sample preparation	70
4.3	Results of directional tunneling spectroscopy	71
4.3.1	Doping dependence of the pairing symmetry and pairing potential	71
4.3.2	Impurity effect	77
4.4	Discussion	78
4.4.1	Pairing symmetry	78
4.4.2	Spatial spectral homogeneity, pseudogap, and competing orders	81
4.4.3	Satellite features	85
4.4.4	Quantum impurities	86
4.5	Summary	87

5 Tunneling Spectra of Electron-Doped $\text{Sr}_{1-x}\text{La}_x\text{CuO}_2$	88
5.1 Introduction	88
5.2 Crystalline structure and sample preparation	91
5.3 Results of scanning tunneling spectroscopy	92
5.3.1 Pairing symmetry and pairing potential of pure $\text{Sr}_{1-x}\text{La}_x\text{CuO}_2$	94
5.3.2 Spectral characteristics of pure $\text{Sr}_{1-x}\text{La}_x\text{CuO}_2$	96
5.3.3 Tunneling spectra of Zn- and Ni-doped $\text{Sr}_{1-x}\text{La}_x\text{CuO}_2$	98
5.4 Discussion	102
5.4.1 Pairing symmetry	102
5.4.2 Impurity substitution and pairing symmetry	103
5.4.3 Satellite features, pseudogap phenomena, and competing orders	105
5.4.4 Low-energy excitations, quantum fluctuations, and quantum criticality	108
5.5 Summary	110
6 Competing Orders, Quantum Phase Fluctuations, and Quasiparticle Tunneling Spectra	111
6.1 Introduction	111
6.2 Competing orders and quantum phase fluctuations on low-energy excitations	113
6.2.1 Formalism	114
6.2.2 Numerical results	117
6.2.3 Summary	122
6.3 Collective modes and quasiparticle interference on the local density of states of cuprate superconductors	123
6.3.1 Model	123
6.3.2 Numerical results	127
6.3.3 Summary	131
6.4 Conclusion	131

Conclusion	134
Appendices	135
A Blonder-Tinkham-Klapwijk Formalism	136
B Tip Preparation, Piezo Calibration, and Thermal Drifting	141
B.1 Tip preparation	141
B.2 Piezo calibration and HOPG images	142
B.3 Thermal drifting calibration and gold images	143
C Modeling the STS data in the presence of impurities	146

List of Figures

1.1	Crystalline structures of three representative cuprates	2
1.2	The zero-field temperature (T) vs. doping (x) phase diagram	4
1.3	Schematic diagram of a single CuO_4 cluster	7
1.4	Order parameter of d and $(d + s)$ -pairing symmetry	10
1.5	Nernst region and the pseudogap phase	12
2.1	Schematic diagram of scattering processes at the N-I-S interface	34
2.2	Momentum dependence of a d -wave pairing potential	36
2.3	Simulated tunneling spectra of a d -wave superconductor	37
2.4	Trajectories of the Andreev bound states	38
2.5	Tunneling spectra along the $\{110\}$ -axis for various pairing symmetries	39
2.6	Tunneling spectra along the c -axis for various pairing symmetries	40
3.1	Schematic diagram of an STM system	45
3.2	Schematic diagram of STM coarse movement control	46
3.3	Schematic diagram of the STM head	48
3.4	Principle of the coarse approach mechanism	49
3.5	Schematic diagram of the STM feedback controller	51
3.6	Schematic diagram of the sequential triggering circuit	52
3.7	Schematic diagram of the STM cryogenic probe	54
3.8	Transmitted vibrational noise spectra	57
3.9	Low-frequency acoustic noise spectra	58

3.10	Transmission of the cryogenic microwave powder filter.	59
4.1	The generic phase diagram of the hole-doped cuprate superconductors	68
4.2	Spatially resolved (dI_{NS}/dV) vs. V spectra of YBCO	72
4.3	Normalized (dI_{NS}/dV) vs. V spectra of YBCO	73
4.4	Normalized tunneling spectra of YBCO and BTK fitting curves	74
4.5	Representative c -axis tunneling spectra of YBCO	75
4.6	Normalized c -axis tunneling spectra of impurity-doped YBCO	77
4.7	YBCO c -axis tunneling spectra near a non-magnetic impurity	78
4.8	Numerical simulation of $\{110\}$ tunneling spectra for various pairing symmetries	79
4.9	Doping dependence of the spectral gap Δ_d and $2\Delta_d/k_B T_c$ ratio in YBCO	83
5.1	Comparison of the crystalline structures	92
5.2	Representative surface topography of pure SLCO	93
5.3	Representative quasiparticle tunneling spectra of SLCO	95
5.4	Temperature dependence of the spectral gap in SLCO	97
5.5	Current dependence of tunneling spectra in SLCO	97
5.6	Tunneling spectra of Zn-SLCO	99
5.7	Tunneling spectra of Ni-SLCO	100
5.8	The spatial evolution of the spectral difference	101
5.9	Tunneling spectra of anisotropic s -wave pairing	102
5.10	Magnetic susceptibility data of pure and impurity doped SLCO	104
5.11	Current-induced pseudogap in SLCO	107
5.12	Vortex phase diagram of SLCO	108
5.13	Field-induced quantum phase transition	109
6.1	Ring diagram and Dyson's equation	116
6.2	Calculated quasiparticle DOS: s -wave electron-doped cuprates	118
6.3	Spectral evolution with V/Δ for s -wave superconductors	120

6.4	Calculated quasiparticle DOS: <i>d</i> -wave hole-doped cuprates	121
6.5	Model of the pinned density waves	124
6.6	Calculated energy-dependent FT-LDOS: non-magnetic impurities	128
6.7	Evolution of the relative intensities of FT-LDOS with energy	129
6.8	Calculated energy-dependent FT-LDOS: pinned SDW	130
6.9	Calculated real space LDOS modulations	131
6.10	Calculated temperature-dependent FT-LDOS	132
A.1	Schematic diagram of energy vs. momentum at N-S interface	138
A.2	Differential tunneling conductance vs. bias voltage for various barrier heights	140
B.1	SEM images of STM tips	142
B.2	STM topographic images of highly ordered pyrolytic graphite	142
B.3	The temperature dependence of the piezo coefficient	143
B.4	Comparison of STM images before and after tip re-approach	144
B.5	STM topographic images of gold at various temperatures	145